



Review

Recent Advances in LDH/g-C₃N₄ Heterojunction Photocatalysts for Organic Pollutant Removal

Cheng Du ^{1,2}, Jialin Xu ^{1,2}, Guixiang Ding ³, Dayong He ^{1,2}, Hao Zhang ², Weibao Qiu ¹, Chunxue Li ⁴ and Guangfu Liao ^{1,3,*}

¹ Shenzhen Institute of Advanced Technology, Chinese Academy of Sciences, Shenzhen 518055, China; duch3@mail3.sysu.edu.cn (C.D.); xujialin@mindray.com (J.X.); kaneh1994@163.com (D.H.); wb.qiu@siat.ac.cn (W.Q.)

² Shenzhen Mindray Bio-Medical Electronics Co., Ltd., Shenzhen 518000, China; zhanghao_e@mindray.com

³ College of Materials Engineering, Fujian Agriculture and Forestry University, Fuzhou 350002, China; dgx421148676@yeah.com

⁴ College of Ecological Environment and Urban Construction, Fujian University of Technology, Fuzhou 350118, China; chunxueli@fjut.edu.cn

* Correspondence: liaogf@mail2.sysu.edu.cn

Abstract: Environmental pollution has been decreased by using photocatalytic technology in conjunction with solar energy. An efficient method to obtain highly efficient photocatalysts is to build heterojunction photocatalysts by combining graphitic carbon nitride (g-C₃N₄) with layered double hydroxides (LDHs). In this review, recent developments in LDH/g-C₃N₄ heterojunctions and their applications for organic pollutant removal are systematically exhibited. The advantages of LDH/g-C₃N₄ heterojunction are first summarized to provide some overall understanding of them. Then, a variety of approaches to successfully assembling LDH and g-C₃N₄ are simply illustrated. Last but not least, certain unmet research needs for the LDH/g-C₃N₄ heterojunction are suggested. This review can provide some new insights for the development of high-performance LDH/g-C₃N₄ heterojunction photocatalysts. It is indisputable that the LDH/g-C₃N₄ heterojunctions can serve as high-performance photocatalysts to make new progress in organic pollutant removal.

Keywords: layered double hydroxides; carbon nitride; heterojunction; photocatalysis; organic pollutant removal



Citation: Du, C.; Xu, J.; Ding, G.; He, D.; Zhang, H.; Qiu, W.; Li, C.; Liao, G. Recent Advances in LDH/g-C₃N₄ Heterojunction Photocatalysts for Organic Pollutant Removal.

Nanomaterials **2023**, *13*, 3066. <https://doi.org/10.3390/nano13233066>

Academic Editor: Antonino Gulino

Received: 30 October 2023

Revised: 28 November 2023

Accepted: 30 November 2023

Published: 1 December 2023



Copyright: © 2023 by the authors. Licensee MDPI, Basel, Switzerland. This article is an open access article distributed under the terms and conditions of the Creative Commons Attribution (CC BY) license (<https://creativecommons.org/licenses/by/4.0/>).

1. Introduction

Environmental pollution has made it extremely difficult for humanity to flourish sustainably [1–5]. The use of photocatalytic technology to harness clean and reproducible solar energy is widely considered to be the most effective answer to the issues [6–8]. An effective method for reducing pollution is to use photocatalytic technology to degrade organic pollutants by using solar irradiation [9,10]. In principle, photocatalysis is an oxidation-reduction process. The fundamental components of the photocatalytic process, photocatalysts, are crucial in driving the reaction and harvesting light [11–15]. Consequently, research into highly effective photocatalysts is crucial for the advancement of photocatalytic technology.

An organic semiconductor having triazine or heptazine as its main constitutional unit and a layer structure resembling graphite is known as graphitic carbon nitride (g-C₃N₄) [7,8,16]. Since the use of g-C₃N₄ in photocatalytic hydrogen synthesis was initially discovered [17], it has garnered considerable interest. Because g-C₃N₄ possesses a smaller band gap (approximately 2.7 eV) than traditional photocatalysts like TiO₂ [18], it can be stimulated by visible light. Furthermore, g-C₃N₄ is competitive among other photocatalytic materials due to its excellent chemical stability, high thermostability, affordable raw ingredients, and straightforward production procedure [19–22]. However, there are numerous issues with the industrial uses of g-C₃N₄. Only blue and purple lights, with a wavelength of

460 nm, may pass through g-C₃N₄, resulting in a low solar energy utilization rate [23]. The redox capacity of g-C₃N₄ is reduced because of the rapid recombination of photocarriers. The specific surface area (SSA) of g-C₃N₄ is relatively tiny because of its bulk characteristics. These flaws prevent g-C₃N₄ from being developed further for photocatalytic uses. To increase the photocatalytic performance of g-C₃N₄, various techniques have been used, including decorating co-catalysts, doping elements (such as F, O, Ni, Fe, etc.), building nanostructures, creating heterojunctions [24,25], etc. To boost the separation of charge carriers in g-C₃N₄, creating heterostructures with different semiconductors is the most important technique. Because of the varying Fermi levels between various photocatalysts, when they come into contact with one another, charge carriers can travel across the semiconductors, which ultimately create an internal electric field (IEF) between them. The electric field allows the photoinduced electrons and holes to flow in a certain direction, thereby separating them [26,27].

A highly efficient method for improving photocatalytic performance has recently been discovered by creating layered double hydroxides (LDHs)/g-C₃N₄ heterojunctions. Essentially, LDHs are a class of two-dimensional (2D) hydrotalcite-like clay materials made up of exchangeable interlayer anions and positively charged host layers [28,29]. LDHs and their derivatives have been found useful in a variety of sectors, especially photocatalysis, because of their inexpensive features, excellent chemical stability, customizable composition, homogeneous distribution of cations and anions, and interchangeable interlayer anions. Nevertheless, because of the fast recombination of photocarriers, the photocatalytic activity of single LDHs is unsatisfactory [30]. Therefore, by building LDH/g-C₃N₄ heterojunctions with a smart design, it is possible to obtain optimal photocatalysts with top performance while overcoming the drawbacks of g-C₃N₄ and LDHs.

Until now, although there have been numerous encouraging reviews on g-C₃N₄ and LDH-based photocatalysts [7,26,27,29,31–34], a comprehensive review specifically focusing on LDH/g-C₃N₄ heterojunctions for organic pollutant removal is unavailable. In this review, recent developments in LDH/g-C₃N₄ heterojunctions and their applications for organic pollutant removal are carefully reviewed. The advantages of LDH/g-C₃N₄ heterojunctions are first summarized to provide some overall understanding of them. Then, a variety of approaches to successfully assembling LDHs and g-C₃N₄ are simply illustrated. Last but not least, certain unmet research needs for the LDH/g-C₃N₄ heterojunction are suggested. This review can provide some new insights for the development of high-performance LDH/g-C₃N₄ heterojunction photocatalysts. It is indisputable that the LDH/g-C₃N₄ heterojunctions can serve as high-performance photocatalysts to make new progress toward organic pollutant removal.

2. Advantages of LDH/g-C₃N₄ Heterojunctions

It has been suggested that one efficient method to enhance the photocatalytic activity of LDH/g-C₃N₄ composites is to build 2D/2D heterojunctions. In addition to providing a large number of surface active sites to create heterojunctions, the 2D structure of LDHs and g-C₃N₄ significantly reduces the distance over which photocarriers must move within the 2D/2D heterojunctions, favoring a photocatalytic reaction [35,36]. LDHs are ideal materials for creating 2D/2D heterojunctions with g-C₃N₄ because of their suitable band structure and variable composition [29]. As is known to all, the band gap of LDHs is about 2.0–3.4 eV, which can be adjusted by changing and regulating the M²⁺ and M³⁺, which is advantageous for the capture of visible light [37]. In addition, the materials' abundance of basic sites makes them useful as heterogeneous photocatalysts for various chemical processes [38]. The active sites of LDH/g-C₃N₄ 2D/2D heterojunctions are also changeable due to the ability to manipulate the cations and anions [39]. Moreover, designing LDHs' interlayer space, number of layers, and functionalization with g-C₃N₄ are all rather simple processes (Figure 1). There are several advantages to LDH/g-C₃N₄ heterojunctions as shown below: (i) Owing to the close contact between LDHs and g-C₃N₄, photocarriers can conveniently migrate, which is beneficial for photocarrier separation [40]. (ii) The high surface area in

LDH/g-C₃N₄ heterojunctions and their strong light harvesting ability are beneficial for photocatalytic activity [41]. (iii) LDH/g-C₃N₄ heterojunctions exhibit a shorter migration distance than photocarriers, thus reducing the electron-hole recombination [42]. (iv) The band structure can be simply adjusted [43]. All of these advantages ensure them with huge application potential in organic pollutant removal.

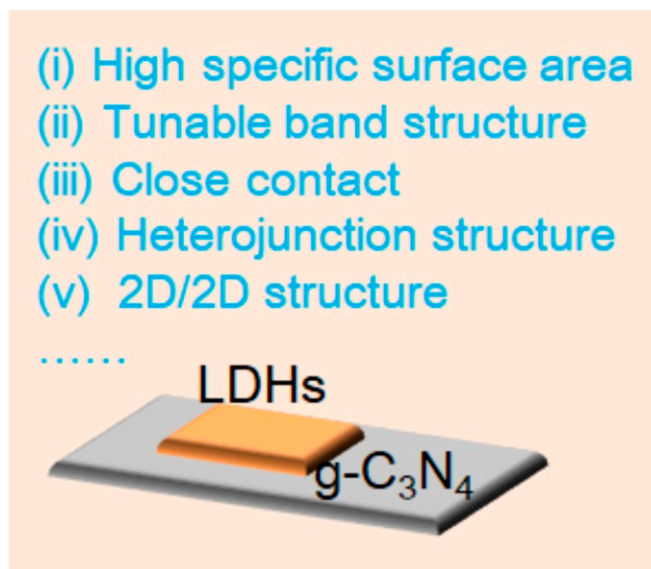


Figure 1. Advantages of LDH/g-C₃N₄ heterojunctions.

Based on the band alignment between the conduction band (CB) and the valence band (VB) of LDHs and g-C₃N₄, the heterojunctions formed between them can be classified into three types: straddling-gap junctions (Type I), staggered-gap junctions (Type II), and broken-gap junctions (Type III). When two semiconductors with staggered band alignment are intimately contacted, and there exists a charge migration between the CB in LDHs and the VB in g-C₃N₄, a Z-scheme system is formed. This Z-scheme system is characterized by an efficient electron-hole separation process, leading to enhanced photocatalytic activity. The charge transfer between the semiconductors results in the formation of a potential difference at the interface, driving the separation of photogenerated charge carriers and reducing their recombination rate. This mechanism significantly improves the overall efficiency and performance of the heterojunction photocatalysts. Therefore, understanding the band alignment and charge transfer processes in heterojunction systems is crucial for the design and optimization of advanced photocatalytic materials with superior performance. Although both the Z-scheme and Type II heterojunctions have the same staggered band alignment, e⁻-h⁺ transfer occurs in opposite directions in these two semiconductors. In contrast to Type II heterojunctions, where photogenerated e⁻ and h⁺ are transferred from high potentials to low potentials, leading to compromised redox capacities, a Z-scheme heterojunction can drive the photogenerated e⁻ in LDHs to migrate and then recombine with the photogenerated h⁺ in g-C₃N₄. This process leaves the high energy h⁺ at the VB of LDHs and the high energy e⁻ at the CB of g-C₃N₄ for photocatalysis [44].

To confirm the existence of the type of heterojunction, band structure analysis is crucial [45]. The solid UV-vis absorption and the X-ray photoelectron spectroscopy (XPS) valence band spectrum are common techniques for obtaining the band structure. Through the band structure analysis, we can determine what kind of heterojunction it is (Type I, Type II, and Type III). Notably, Type II and Z-scheme heterojunctions share a similar staggered band alignment structure. Nevertheless, their charge transfer pathways are significantly different. In order to determine if the charge transfer route is Z-scheme or type II heterojunctions, it is therefore critically necessary to investigate it in detail using some techniques such as (i) self-confirmation by photocatalytic reactions, products,

and radical species, (ii) selective photodeposition of a noble metal, (iii) in situ XPS, (iv) femto-second transient absorption spectra (fs-TAS), (v) photoassisted Kelvin probe force microscopy (photo-KPFM), theoretical calculations, etc. For example, the work function (Φ) plays a crucial role in investigating the energy band alignment and charge transfer of heterojunctions, making it an essential physical parameter [46]. We can also determine Φ through theoretical calculations and further determine the charge transfer route.

3. Synthetic Strategy of LDH/g-C₃N₄ Heterojunctions

To obtain good photocatalytic performance, the development of the LDH/g-C₃N₄ heterojunctions is crucial. The principal building techniques, such as electrostatic self-assembly, in situ coprecipitation, hydrothermal, solvothermal, and calcination strategies, depend on the assembly strategies of LDHs and g-C₃N₄. These synthesis techniques are covered in depth in the sections that follow.

3.1. Electrostatic Self-Assembly Method

Layered composites are frequently manufactured via electrostatic self-assembly. It utilizes the electrostatic interactions between materials with various charges [47–49]. During the self-assembly process, the electrostatic adsorption with different charges mainly propels the assembly, while electrostatic repulsion between like charges controls the assembly of each layer. In contrast to the electropositive host layer of the LDHs created by the orderly arrangement of metal cations, the suspension of virgin g-C₃N₄ in aqueous solution is electronegativity due to –NH₂ deprotonation [50,51]. By means of electrostatic self-assembly, LDH/g-C₃N₄ heterojunctions can be produced thanks to these characteristics. LDHs and g-C₃N₄ are exfoliated to nanosheets during the synthesis process before self-assembly. There are numerous ways to exfoliate LDHs using mechanical stirring or ultrasonic treatment [52]. For example, Tahir and co-workers reported 2D/2D CoAl-LDH/g-C₃N₄ heterojunctions with a strong interface through the self-assembled deposition of CoAl-LDH flakes onto layered g-C₃N₄ nanosheets (Figure 2) [53]. They further used the CoAl-LDH/g-C₃N₄ product for MDR and methane bi-reforming to reduce flared gas (methane) with CO₂. Mg-Al-LDH/g-C₃N₄ materials were created by Xu and co-workers using an electrostatic self-assembled method. In this work, the scientists initially produced Mg-Al-LDH through deposition with NaOH and g-C₃N₄ from urea by thermal polymerization. Then, g-C₃N₄ nanosheets and Mg-Al-LDH nanosheets were created using a combination of the hydrothermal method and sonication exfoliation. The produced g-C₃N₄ and Mg-Al-LDH showed zeta potentials of 27.3 mV and 52.7 mV, respectively. The Mg-Al-LDH/g-C₃N₄ photocatalyst was produced by immediately combining the two photocatalysts, which caused the g-C₃N₄ and Mg-Al-LDH to electrostatically interact with each other. The scientists used a transmission electron microscope (TEM) to examine the photocatalyst morphology in order to confirm the 2D/2D assembly of Mg-Al-LDH and g-C₃N₄ and discovered that Mg-Al-LDH flakes were evenly distributed onto g-C₃N₄ sheets.

3.2. In Situ Coprecipitation Strategy

By introducing a precipitating agent, the synchronous precipitation of more than one cation in a uniform solution is known as coprecipitation. Because of the straightforward manipulation, cheap and controllable reaction circumstances, and homogeneous composition, this technology has been a significant means of preparing composites with two or multiple metals [10,54,55]. The process of coprecipitation is also frequently utilized to create LDHs [56]. By combining the metal cations needed for the host layer with alkaline liquor, and then allowing the suspension to age, the necessary LDHs can be produced. The interlayer anions of the LDHs are present in the mixed cationic solution. By adjusting the reaction parameters, e.g., solution pH, temperature, and aging time, the LDH size can be tailored. The basic process for generating LDH/g-C₃N₄ through coprecipitation involves depositing the metal cations on the g-C₃N₄ nanosheet once they have been electrostatically deposited onto it.

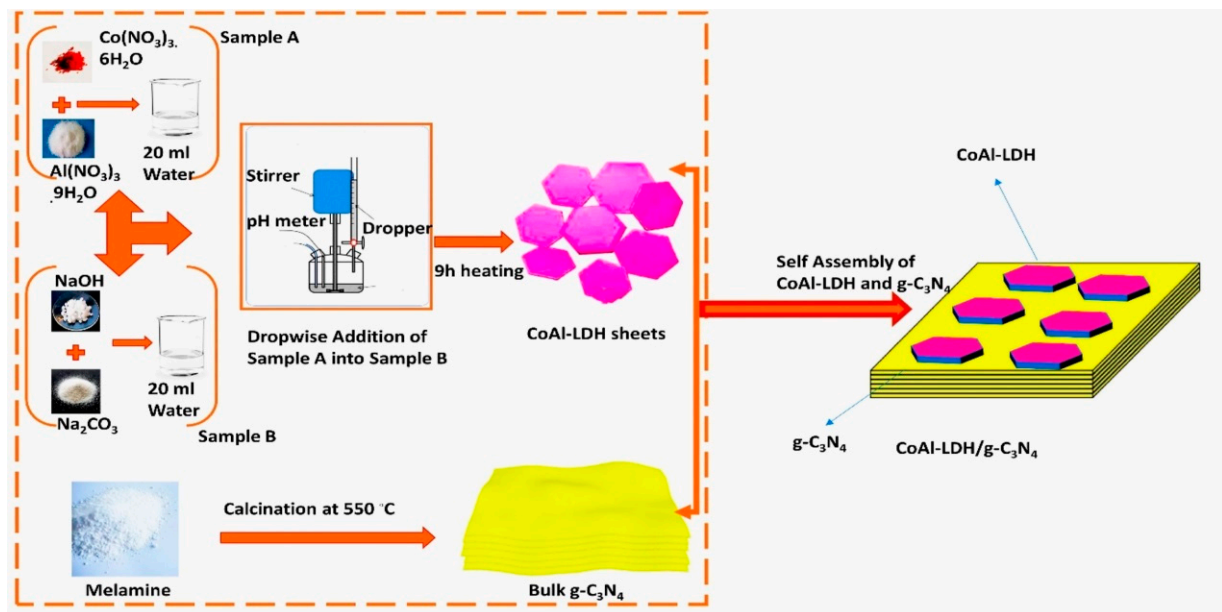


Figure 2. Schematic illustration of the synthesis of CoAl-LDH, $\text{g-C}_3\text{N}_4$, and CoAl-LDH/ $\text{g-C}_3\text{N}_4$ composite samples. Reproduced with permission [53].

By using in situ coprecipitation, Li and colleagues [57] have successfully created a 2D/2D Zn-Cr-LDH/ $\text{g-C}_3\text{N}_4$ heterojunction. Figure 3 depicts the precise synthesis procedure (from I to V). The modified $\text{g-C}_3\text{N}_4$ sheets, also known as $\text{g-C}_3\text{N}_4\text{-C(N)}$ sheets, were originally created by the authors by combining urea with citric acid. They were then formed into a suspension. Through electrostatic attraction, Zn^{2+} and Cr^{3+} were deposited onto the $\text{g-C}_3\text{N}_4\text{-C(N)}$ nanosheet during this procedure. After that, NaOH was used for depositing Zn^{2+} and Cr^{3+} to create Zn-Cr-LDH on the surface of $\text{g-C}_3\text{N}_4$. The photocatalytic activity of the Zn-Cr-LDH/ $\text{g-C}_3\text{N}_4\text{-C(N)}$ product used by the authors to further photocatalyze the breakdown of Congo red was obviously higher than Zn-Cr-LDH or $\text{g-C}_3\text{N}_4$ alone. An in situ crystallization technique, used to create Zn-Al-LDH/ $\text{g-C}_3\text{N}_4$ composites, was disclosed by Yuan and co-workers [58]. In this work, Zn^{2+} and Al^{3+} coprecipitated to in situ produce Zn-Al-LDH crystals on $\text{g-C}_3\text{N}_4$ nanosheets. The microstructure of Zn-Al-LDH/ $\text{g-C}_3\text{N}_4$ was studied by using TEM, and they discovered the comparatively large $\text{g-C}_3\text{N}_4$ nanosheets were homogeneously coated on Zn-Al-LDH flakes.

3.3. Hydrothermal Strategy

The hydrothermal strategy is a popular method to create composites at high temperatures and high pressures in a pressure-tight reactor by using water as a solvent [59–62]. The fundamental benefit of this technology is the ease with which a crystalline product can be produced via a straightforward hydrothermal procedure. Controlling the reaction conditions also makes it easy to develop the morphology and structure of materials [63]. The process of hydrothermal oxidation, reduction, precipitation, breakdown, polymerization, and so forth are further subcategories of the hydrothermal method depending on the type of reaction that occurs. Numerous researchers have employed the hydrothermal precipitation approach to create LDH/ $\text{g-C}_3\text{N}_4$ heterostructures. Under mild temperature and pressure circumstances, it can be challenging for some metal cations to coprecipitate and produce layered hydroxides, but in a hydrothermal environment with high temperature and pressure, the reaction is simpler to carry out. Additionally, the LDH/ $\text{g-C}_3\text{N}_4$ products that are produced typically have a nice 2D/2D morphology.

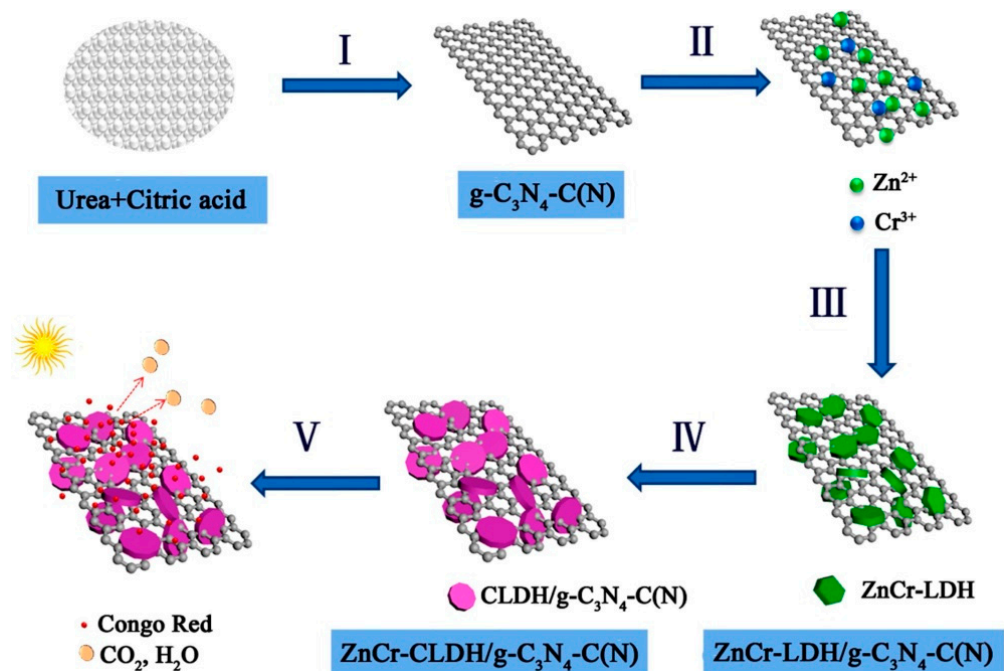


Figure 3. Diagrammatic sketch of the synthesis process and photocatalytic property of ZnCr-CLDH/g-C₃N₄-C(N). (I) Thermal polymerization at 550 °C, (II) introduction of Zn²⁺ and Cr³⁺ under the condition of continuous stirring, (III) in situ precipitation of ZnCr-LDH on g-C₃N₄-C(N), (IV) calcination and then formation of ZnCr-CLDH/g-C₃N₄-C(N); (V) adsorption and photocatalytic performance for CR removal under visible light irradiation. Reproduced with permission [57].

By using a hydrothermal process, Liu and colleagues [64] have created a Zn-Cr-LDH/g-C₃N₄ composite (Figure 4). In their research, bulk g-C₃N₄ was made via thermal polymerization using urea as precursors, and was treated with ultrasound to produce a g-C₃N₄ nanosheet suspension. The suspension was then mixed with Zn²⁺, Cr³⁺, and lye. The hydrothermal reaction was carried out for 24 h under 120 °C. The precipitates from the autoclave were eventually collected and dried to produce the Zn-Cr-LDH/g-C₃N₄. Chew and co-workers [65] employed urea and NH₄F instead of NaOH lye for the hydrothermal preparation of Co-Al-LDH/O-doped g-C₃N₄ in order to create LDH/g-C₃N₄ with uniform 2D/2D morphology. In order to prevent the nonuniform precipitant dispersion and response rate from causing unequal LDH sizes, Co²⁺ and Al³⁺ were precipitated in this technique using the hydrolysis of urea. The hydrolysis of urea produced NH₃ and CO₂. While the release of CO₂ served to agitate the reaction mixture, the produced NH₃ raised the pH value. As a result, Co-Al-LDH flakes eventually precipitated in a homogenous fashion, further producing high-purity products of consistent size.

3.4. Solvothermal Method

The hydrothermal process is improved upon by the solvothermal method. Organic solvents are used as the reaction medium. Although the hydrothermal approach has numerous benefits, it is only capable of producing a small number of non-oxides, such as carbides, nitrides, and phosphides, because both the reactants and the products can hydrolyze or react with H₂O [32,66,67]. Nonaqueous solvents can be used to properly execute these reactions. Additionally, under high-pressure conditions, several organic solvent properties, such as density, viscosity, and surface tension, fluctuate greatly, which can create specialized media for numerous chemical processes [68]. Due to some organic solvents' lower boiling points, the gas pressure in solvothermal systems can be higher than that in hydrothermal systems at the same temperature, and the higher pressure encourages the crystallization of the product [69]. When building the LDH/g-C₃N₄ heterostructure, an organic solvent

can increase the reaction precursors' dispersity (for instance, a $g\text{-C}_3\text{N}_4$ suspension), which boosts their chemical reactivity and makes it easier to build 2D/2D structures. Given the benefits, the solvothermal approach was frequently used in investigations to create LDH/ $g\text{-C}_3\text{N}_4$ photocatalysts.

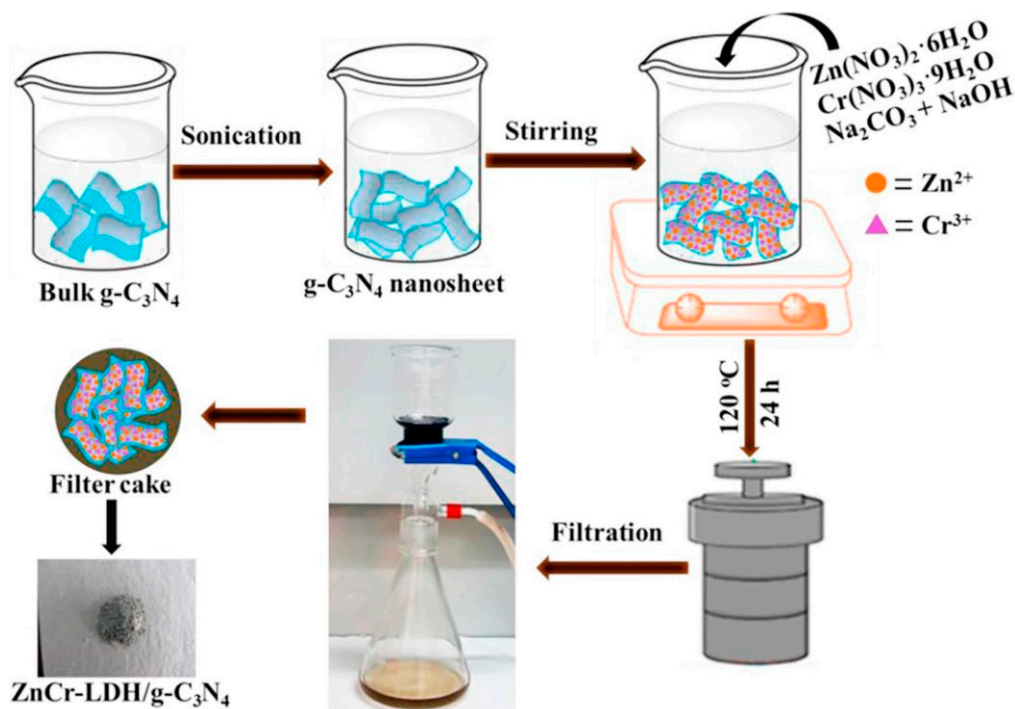


Figure 4. Representative synthesis process of ZnCr-LDH/ $g\text{-C}_3\text{N}_4$. Reproduced with permission [64].

Recently, Zhao and co-workers [70] have created Zn-Al-LDH/ $g\text{-C}_3\text{N}_4$ composites using the solvothermal technique (Figure 5). Ethylene glycol (EG) was used as the reaction environment in their research. Through calcining the urea and suspending it in EG with NaOH, $g\text{-C}_3\text{N}_4$ was prepared. The solvothermal procedure then involved combining the two EG suspensions. The TEM observation showed that $g\text{-C}_3\text{N}_4$ sheets were evenly distributed in EG and that the Zn-Al-LDH/ $g\text{-C}_3\text{N}_4$ had a suitable lamellar structure. In addition, it was discovered that the Zn-Al-LDH interlayer spacing (1.03 nm) was greater than ordinary LDHs intercalated with carbonate (0.73 nm). In order to boost photocatalytic efficiency, a comparatively large interlayer spacing can offer larger room for reactant transport and more sites that are active for photosynthesis [71]. Lian and co-workers [72] synthesized a 2D/2D NiCo-LDH/ $g\text{-C}_3\text{N}_4$ Z-scheme heterojunction through the solvothermal technique, which displayed improved photocatalytic efficacy under visible light illumination for the breakdown of tetracycline hydrochloride (TC) and the formation of hydrogen (H_2). For the NiCo-LDH/ $g\text{-C}_3\text{N}_4$, a Z-scheme mechanism was suggested, demonstrating the heterojunction's twin benefits of strong redox capacity.

3.5. Calcination Method

A substance is heated during calcination to cause it to evaporate H_2O . This technique is used to create composites of calcined LDH and $g\text{-C}_3\text{N}_4$. LDHs are utilized as starting materials in the synthesis process, where they are calcined to create mixed metal oxides (MMOs) through geometric modification [73,74]. The produced MMOs exhibit excellent thermal stability and can be widely distributed. The production of metal oxides with an increased specific surface area and porosity allows for the further enhancement of photocatalytic efficiency [75]. Furthermore, calcining LDHs can create spinels, which can improve their capacity to capture visible light [76]. The literature that is currently accessible

indicates that there are three calcination techniques to produce a calcined LDH/g-C₃N₄ heterojunction. First, the produced LDH/g-C₃N₄ composites are immediately calcined. The second technique involves first calcining LDH to MMO and then calcining the compounds of MMO and g-C₃N₄ [77]. The third strategy, which was more often employed, involves co-calcining the raw materials for g-C₃N₄ and LDH [31]. Figure 6 illustrates the synthesis of dual-S-scheme g-C₃N₄/Ti₃C₂T/Co₂Al_{0.95}La_{0.05}-LDH composites through a simple calcination method [78]. Benefits of the g-C₃N₄/Ti₃C₂T/CoAlLa-LDH dual-S-scheme assembly include faster charge transfer between the conductor and semiconductor. Additionally, a simple coprecipitation technique was used to create a nanocomposite with a noteworthy 2D/2D heterojunction made of CoFe-LDH loaded on g-C₃N₄ nanosheets [79]. When compared to pure g-C₃N₄ and CoFe-LDH alone, the prepared nanocomposite showed noticeably higher photocatalytic performance for TC removal.

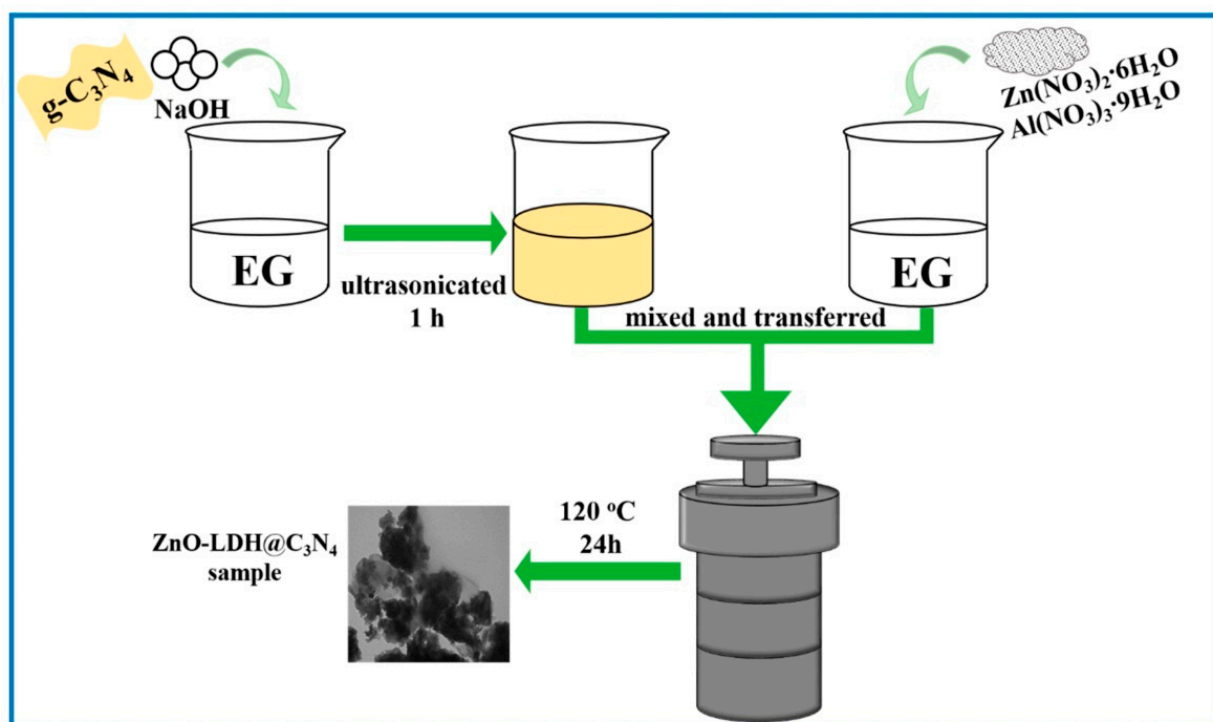


Figure 5. The representative synthesis process of Zn-Al-LDH/g-C₃N₄. Reproduced with permission [70].

Numerous preparation techniques, including electrostatic self-assembly, in situ coprecipitation, hydrothermal, solvothermal, and calcination, are beneficial for achieving a close and robust interface between g-C₃N₄ and LDH, leading to improved photocarrier migration. Powerful interactions between them, such as covalent bonds, ionic bonds, coordination bonds, hydrogen bonds, and van der Waals forces, may eventually form and serve as pathways for charge transfer while enhancing interface interaction. Especially with the electrostatic self-assembled approach, the original architecture may be conserved and a closely touching interface can be formed. They can be guaranteed to have a homogeneous architecture and small size distribution by using a self-assembly technique. On the other hand, the calcination approach results in a low photocatalytic activity due to the comparatively inadequate interface contact between them. But it is simple and cheap and more suitable for actual industrial production (Table 1).

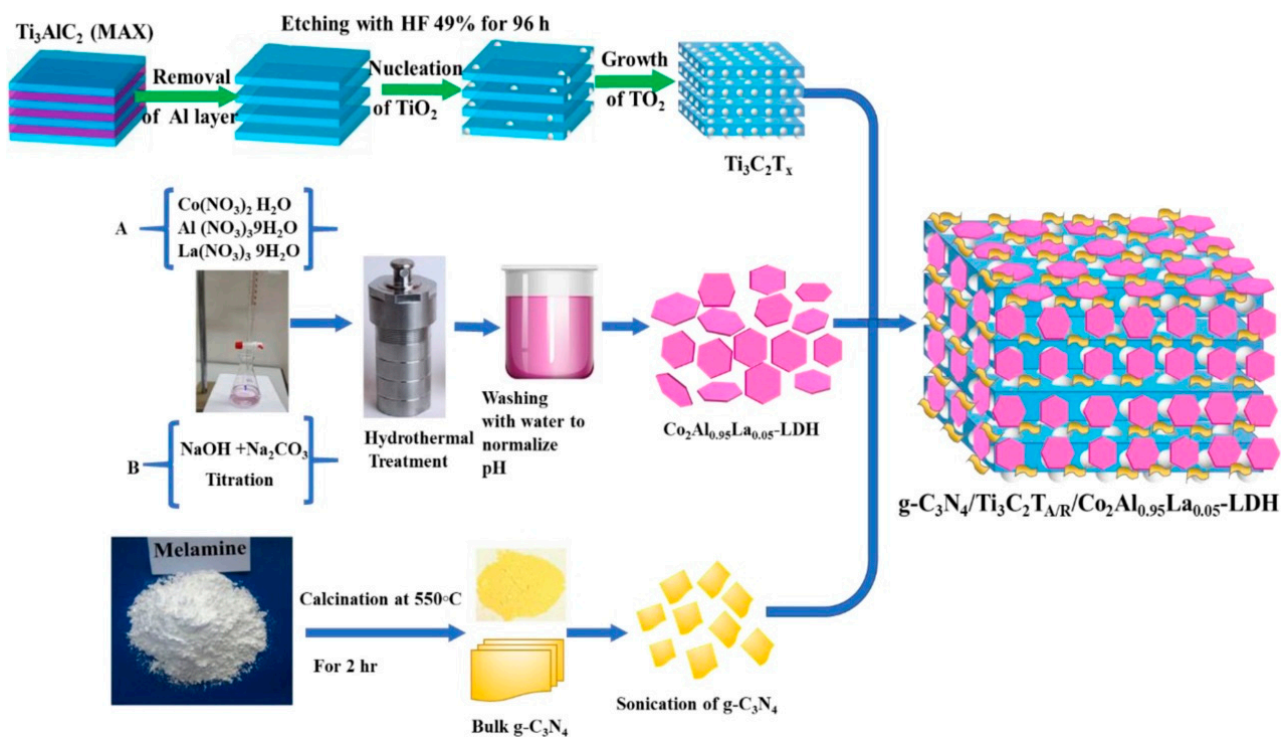


Figure 6. Schematic representation of the synthesis process of $g\text{-C}_3\text{N}_4/\text{Ti}_3\text{C}_2\text{T}/\text{Co}_2\text{Al}_{0.95}\text{La}_{0.05}\text{-LDH}$ composite. Reproduced with permission [78].

Table 1. Comparison between different methods for the preparation of LDH/ $g\text{-C}_3\text{N}_4$ heterojunctions.

| Synthesis Strategy | Advantages | Disadvantages |
|--------------------------------------|---|---|
| Electrostatic self-assembly method | Very suitable for the preparation of 2D/2D LDHs/ $g\text{-C}_3\text{N}_4$ | Time- and cost-consuming, complicated preparation process, and low efficiency |
| In situ coprecipitation method | Facile, eco-friendly, and highly efficient | Easy to agglomerate |
| Hydrothermal and solvothermal method | (i) Facile, eco-friendly, and highly efficient (ii) Produced photocatalysts with a relatively high crystallinity, small size distribution, and controllable architecture | Complex preparation process |
| Calcination method | Facile, eco-friendly, and effective, and reduced aggregation | Relatively poor interface contacts between two semiconductors |

4. LDH/ $g\text{-C}_3\text{N}_4$ Heterojunctions for Organic Pollutant Removal

Because $g\text{-C}_3\text{N}_4$ and LDHs can create a heterojunction efficiently, it is an unusual approach to increase photocatalytic performance. This is because the as-produced electron-hole pairs are effectively separated. The property of LDH/ $g\text{-C}_3\text{N}_4$ photocatalysts can be significantly enhanced via a rational 2D/2D structure design, allowing for their widespread usage in photocatalytic organic pollution removal. The photocatalytic performance and mechanism of several LDHs/ $g\text{-C}_3\text{N}_4$ are examined and addressed in the section that follows.

Divalent cations such as Co^{2+} , Mg^{2+} , Ni^{2+} , Zn^{2+} , etc. as well as trivalent cations such as Al^{3+} , Cr^{3+} , Fe^{3+} , Mn^{3+} , Ti^{3+} , etc. were employed to build LDH/ $g\text{-C}_3\text{N}_4$ heterojunctions, according to the existing literature. These LDH/ $g\text{-C}_3\text{N}_4$ heterojunctions with improved photocatalytic performance were explored for organic pollutant removal. For instance, the ZnAl-LDH/ $g\text{-C}_3\text{N}_4$ photocatalyst was described by Shanker and colleagues [80] using a microwave-assisted technique. Compared to bare $g\text{-C}_3\text{N}_4$ and ZnAl-LDH photocatalysts, the optimized ZnAl-LDH/ $g\text{-C}_3\text{N}_4$ compound showed the greatest photodegradation rate constant of $1.22 \times 10^{-2} \text{ min}^{-1}$ for ciprofloxacin (CIP). Khataee and co-workers [81] re-

ported a $g\text{-C}_3\text{N}_4/\text{ZnFe}$ LDH binary heterojunction for the photodegradation of tetracycline (TC) with the aid of Oxone. The effective combination of $g\text{-C}_3\text{N}_4/\text{ZnFe}$ LDH/Oxone/UV achieved an evidently improved degradation rate for TC. Thus, it can be also effectively used for the removal of other organic pollutants. Using an easy one-step in situ hydrothermal process, mesoporous $g\text{-C}_3\text{N}_4/\text{Zn-Ti}$ LDH-laminated van der Waals heterojunctions were effectively produced [82]. A laminated van der Waals heterostructure was successfully generated between the electronegative $g\text{-C}_3\text{N}_4$ nanocrystal and the electropositive Zn-Ti LDH, thanks to a strong electrostatic attraction between them. As a result, the resulting heterojunctions demonstrated superior photocatalytic performance for eliminating ceftriaxone sodium completely (>97%). This simple method for creating mesoporous $g\text{-C}_3\text{N}_4/\text{Zn-Ti}$ LDH-laminated van der Waals heterojunctions provides new information for creating high-performing photocatalytic materials.

Cerium (Ce) has been widely used as a dopant in LDHs/ $g\text{-C}_3\text{N}_4$ because of its low price and outstanding redox performance [83,84]. Xu and co-workers [85] reported various $g\text{-C}_3\text{N}_4/\text{Ce}$ -doped MgAl-LDHs via a solvothermal strategy (Figure 7a). $g\text{-C}_3\text{N}_4/\text{MgAl}_{0.80}\text{Ce}_{0.20}$ -LDH has a large SSA ($52.71\text{ m}^2\text{ g}^{-1}$) and a good separation efficiency of photocarriers, owing to the coupled effect of Ce-doping and $g\text{-C}_3\text{N}_4$ -LDH heterojunctions (Figure 7b,c). As a result, ~49% Congo red (CR) is adsorbed through $g\text{-C}_3\text{N}_4/\text{MgAl}_{0.80}\text{Ce}_{0.20}$ -LDH, and the CR degradation efficiency reaches 90% within 180 min (Figure 7d,e). They also found that both photogenerated h^+ and superoxide radical $\cdot\text{O}_2^-$ could obviously improve photocatalytic CR oxidation performance (Figure 7e). A more effective transfer of photocarriers between $g\text{-C}_3\text{N}_4$ and $\text{MgAl}_{0.80}\text{Ce}_{0.20}$ -LDH is likely the cause of the enhanced photocatalytic property.

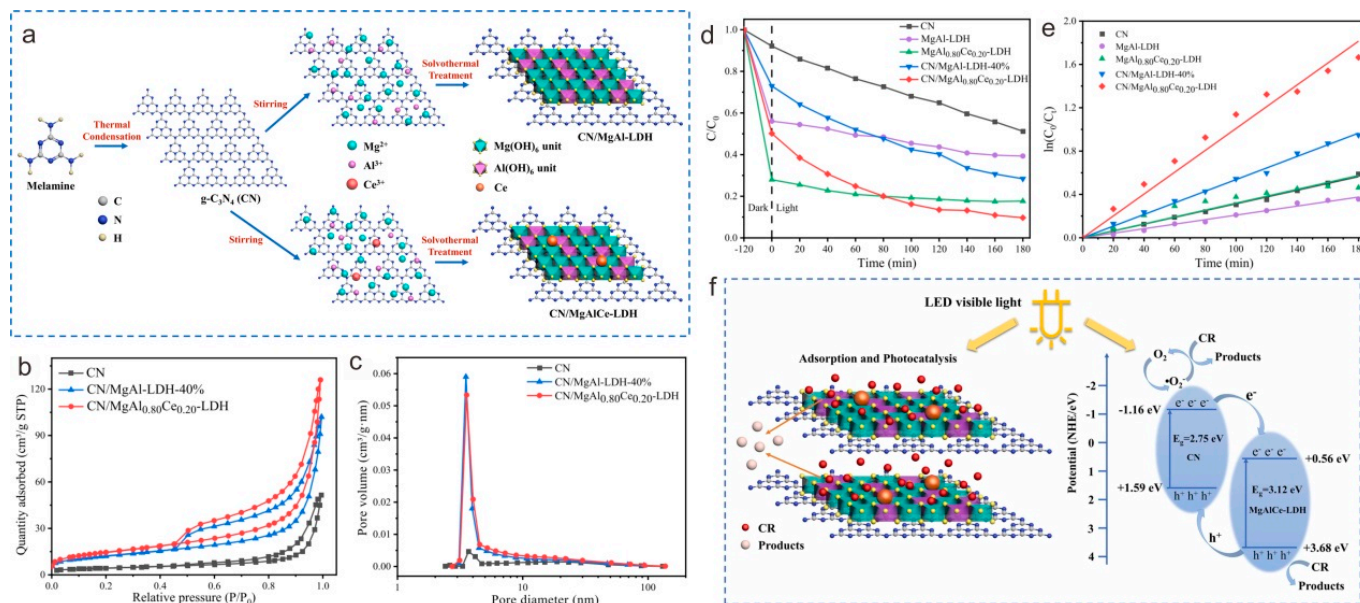


Figure 7. (a) Diagrammatic sketch of fabrication route of $g\text{-C}_3\text{N}_4/\text{MgAl}_{0.80}\text{Ce}_{0.20}$ -LDH. BJH N_2 adsorption-desorption isotherms (b) and pore size distribution (desorption) (c) of $g\text{-C}_3\text{N}_4$ and $g\text{-C}_3\text{N}_4/\text{Ce}$ -doped MgAl-LDHs. CR adsorption capacity (d) and pseudo-first-order kinetic plots for CR photodegradation (e) of $g\text{-C}_3\text{N}_4$ and $g\text{-C}_3\text{N}_4/\text{Ce}$ -doped MgAl-LDHs. (f) Mechanism explanation of photocatalytic degradation via $g\text{-C}_3\text{N}_4/\text{Ce}$ -doped MgAl-LDHs. Reproduced with permission [85].

Dai and co-workers [41] reported $g\text{-C}_3\text{N}_4/\text{Ni-Ti}$ LDH nanocomposites with a high SSA through hydrothermal strategy. These nanocomposites were utilized for the sonophotocatalytic removal of amoxicillin (AMX). The results showed that when AMX is photocatalytically degraded under visible light irradiation, $g\text{-C}_3\text{N}_4/\text{Ni-Ti}$ LDH nanocomposites perform better than their individual $g\text{-C}_3\text{N}_4$ and Ni-Ti LDH. He and his co-workers [86] prepared ZnM-LDH/ $g\text{-C}_3\text{N}_4$ (M = Al, Cr) Z-scheme heterojunctions through the electrostatic

self-assembled strategy. ZnAl-LDH and ZnCr-LDHs/g-C₃N₄ may be desulfurized by photocatalytic oxidation/extraction in 3 h for model oil, with a 99.8 and 96.6% desulfurization rate, respectively. Mahjoub and co-workers [87] reported a new Bi-doped NiAl-LDH/g-C₃N₄ 2D/2D heterojunction for the effective photodegradation of ciprofloxacin (Cipro). Under visible light irradiation, the optimal composite (40%-g-C₃N₄/LDH) demonstrated 86% Cipro elimination effectiveness within 180 min. The enhanced flow of photocarriers to the surface and close face-to-face contact between two semiconductors in heterojunction were the key causes of the aforementioned boost in catalytic activity. This method offers a fresh viewpoint on creating 2D/2D heterojunctions between LDH and other 2D semiconductors for the simultaneous detection and photodegradation of antibiotics.

ZnAl-LDH and a non-metal, boron immersion have been used to structurally modify g-C₃N₄ in order to increase its light absorption. The obtained 40% B-g-C₃N₄ and 30%ZnAl-LDH/g-C₃N₄ displayed an increased SSA of 14.3137 and 26.292 m²/g, illustrating 90.25 and 86.31% phenol photodegradation within 270 min [88]. Lin and co-workers [79] reported a CoFe-LDH/g-C₃N₄ with a notable 2D/2D heterojunction via a simple co-precipitation strategy. When compared to pure g-C₃N₄ and CoFe-LDH, the CoFe-LDH/g-C₃N₄ nanocomposite showed noticeably higher catalytic performance toward TC photodegradation. Jiao and co-workers [89] reported halogen-doping (F and Cl) g-C₃N₄-modified ZnAl-LDH (FCCN/LDH) nanocomposites via a simple coprecipitation process for the photodegradation of TC. In contrast to single FCCN and LDH, the FCCN/LDH showed improved photocatalytic activity, which is because of the proper band alignment and a Z-scheme migration mechanism. The tenable Z-scheme mechanism indicated that the primary free radicals involved in photodegradation are h⁺ and ·O²⁻ active species (Figure 8). In addition, flower-like g-C₃N₄/NiZnAl-LDH S-scheme heterojunctions with oxygen vacancies [90] and vulcanized ZnAl LDH-modified g-C₃N₄ heterojunctions [91] also displayed improved photocatalytic performance.

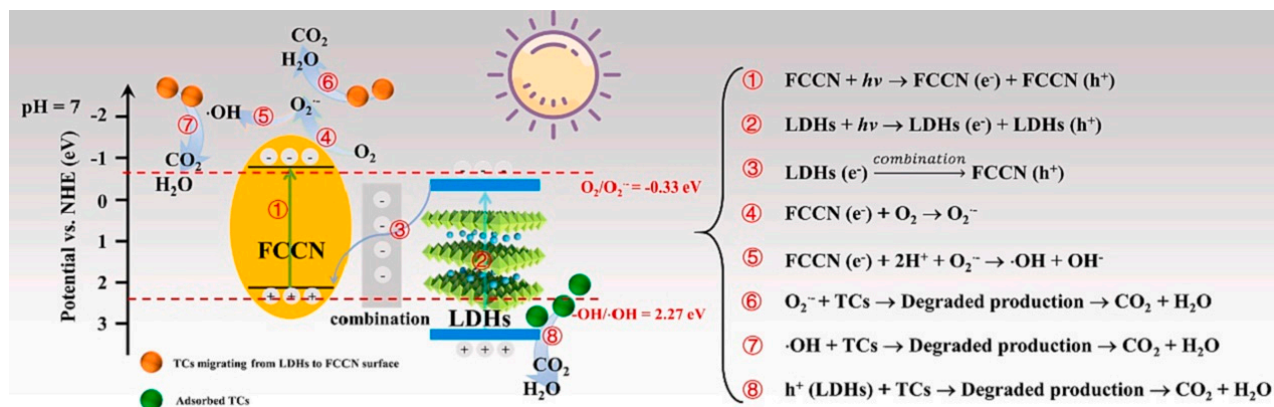


Figure 8. Diagrammatic sketch of FCCN/LDH-100 nanocomposites under visible light illumination. Reproduced with permission [89].

The photocarriers' separation can be increased by connecting LDH and g-C₃N₄, yet some LDH/g-C₃N₄ photocatalysts have charge carriers that are difficult to further migrate and engage in redox processes [92]. Building LDH/g-C₃N₄/X ternary photocatalysts, therefore, needs to be taken into consideration, where X stands for another photocatalyst or noble metal. This plan is anticipated to improve light harvesting and the transfer of photocarriers. Ag and reduced graphene oxide (RGO) were predominantly utilized to achieve these targets, according to the research that is currently available. For instance, Fazaeli et al. [93] prepared a new Ag-bridged dual Z-scheme Ag/g-C₃N₄/CoNi-LDH plasmonic heterojunction by a simple hydrothermal method. The most favorable degradation conditions for a TC solution were found to be 7 pH, 40 g L⁻¹ catalyst dosage, 30 mg L⁻¹ TC concentration, and a 100 min irradiation period. Pazhanivel and co-workers [94] reported

an RGO-supported $g\text{-C}_3\text{N}_4/\text{NiMgAl}$ LDH hybrid for achieving high-performance photocatalytic organic pollution removal. A ternary heterojunction consisting of CoAl -LDH, $g\text{-C}_3\text{N}_4$, and RGO (LDH/CN/RGO) with a noticeable 2D/2D/2D structure utilizing a facile hydrothermal strategy was reported recently [92] (Figure 9a). Of all the manufactured catalysts, the LDH/CN/RGO ternary heterojunction with RGO and LDH contents of 1 weight percent and 15 weight percent, respectively, displayed the highest degrading efficiency (Figure 9b,c). It also showed outstanding stability throughout recycling studies. Due to the unique 2D/2D/2D configuration of the constituent CN, LDH, and RGO, speeding up the photocarriers' transport processes to effectively impede their recombination resulted in enhanced photocatalytic performance (Figure 9d,e). Furthermore, the possible photodegradation routes for both CR and TC were proposed on the basis of the intermediate products (Figure 9f). Therefore, with their high performance and ability to respond to visible light, the current LDH/CN/RGO ternary heterojunctions show great potential for real-world uses in solar energy transformation and environmental preservation.

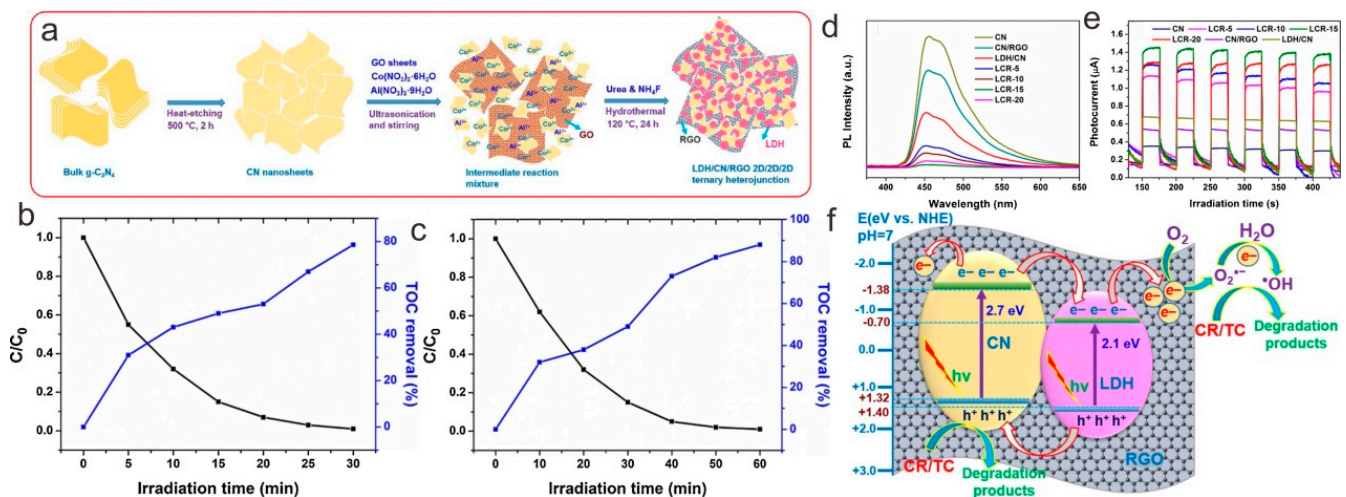


Figure 9. (a) Diagrammatic sketch of the preparation of LDH/CN/RGO 2D/2D/2D heterojunctions. Comparison of the photocatalytic activity and TOC removal rate over the LCR-15 photocatalyst in the photodegradation of CR (b) and TC (c). PL spectra (d) and photocurrent responses (e) of CN, LDH/CN, CN/RGO, and LDH/CN/RGO photocatalysts. (f) Mechanism explanation of photocatalytic degradation of CR and TC over LDH/CN/RGO. Reproduced with permission [92].

Besides the above common LDH/ $g\text{-C}_3\text{N}_4$ heterojunctions, researchers have also made great efforts to develop other candidates to prepare LDH/ $g\text{-C}_3\text{N}_4$ heterojunctions, e.g., NiFe-LDH/ $g\text{-C}_3\text{N}_4$ [95], $g\text{-C}_3\text{N}_4/\text{NiAl-LDH}$ [96], $g\text{-C}_3\text{N}_4/\text{NiFe-LDH}$ [97], $g\text{-C}_3\text{N}_4/\text{MgZnAl-calcined LDH}$ [98], ZnMgAl LTH/ $\text{ZnO}/g\text{-C}_3\text{N}_4$ [99], Co-Al LDH/ $g\text{-C}_3\text{N}_4\text{-CoFe}_2\text{O}_4$ [100], $g\text{-C}_3\text{N}_4/\text{ZnFeMMO}$ [76], $g\text{-C}_3\text{N}_4/\text{LDH/NCQDs}$ [101], NiFe-LDH/NRGO/ $g\text{-C}_3\text{N}_4$ [102], ZnCr-LDH/ $g\text{-C}_3\text{N}_4\text{-C(N)}$ [57], $\text{In}_2\text{S}_3/g\text{-C}_3\text{N}_4/\text{CoZnAl-LDH}$ [103], ZnTi/ $\text{C}_3\text{N}_4/\text{Ag LDH}$ [104], etc. As exhibited in Table 2, $g\text{-C}_3\text{N}_4/\text{Ni-Ti LDH}$ [41] displayed a very high photocatalytic activity by sonophotocatalytic process, and the proposed sonophotocatalytic process and the relatively low cost give them huge application prospects. Furthermore, multicomponent LDH/ $g\text{-C}_3\text{N}_4$ -based photocatalysts such as $\text{CoAl-LDH}/g\text{-C}_3\text{N}_4/\text{RGO}$ [92] displayed some unique merits, and thus it is more worthy of attention. Moreover, for more clarification and improvement, a deeper understanding of the charge migration pathway and the photocatalytic mechanism is essential. Beyond question, LDH/ $g\text{-C}_3\text{N}_4$ systems will have huge potential in photocatalytic organic pollutant removal.

Table 2. Comparison of the photocatalytic organic pollution removal property over LDH/g-C₃N₄ systems.

| Photocatalysts | Preparation Strategy | Mass (mg) | Light Source | Target Pollutant/Initial Concentration | Degradation Time (min) and Rate (%) | K_{app}^a [10^{-2} min^{-1}] | Ref. |
|---|------------------------------------|-----------|-----------------------------------|--|-------------------------------------|--|------|
| ZnAl-LDH/ g-C ₃ N ₄ | Microwave-assisted method | 30 | 35 W Xe arc lamp | CIP/20 mg L ⁻¹ | 140 (~84.1) | 1.22 | [80] |
| g-C ₃ N ₄ / ZnFe LDH | Mechanical stirrer method | 50–300 | 6-W UVC lamp | TC/10–55 μM | 30 (~92.4) | - | [81] |
| g-C ₃ N ₄ / Zn-Ti LDH | Hydrothermal method | 100 | 300 W xenon lamp, >420 nm | Ceftriaxone sodium/10 mg L ⁻¹ | 240 (~97) | 1.14 | [82] |
| g-C ₃ N ₄ / MgAl _{0.80} Ce _{0.20} -LDH | Solvothermal method | 20 | 5 W LED lamp, 400–760 nm | CR/50 mg L ⁻¹ | 180 (~90) | 1.01 | [85] |
| g-C ₃ N ₄ @Ni-Ti LDH | Hydrothermal method | - | 400 W Hg lamp | AMX/1000 mg L ⁻¹ | 75 (~99.5) | - | [41] |
| ZnM-LDH/ g-C ₃ N ₄ (M = Al, Cr) | Electrostatic self-assembly method | 180 | 500 W mercury lamp | Model oil/90 mL | 180 (~99.8) | - | [86] |
| Bi-doped NiAl-LDH/ g-C ₃ N ₄ | Annealing method | 50 | 400 W Mercury-vapor lamp, >400 nm | Cipro/10 mg L ⁻¹ | 180 (~86) | - | [87] |
| ZnAl-LDH/ g-C ₃ N ₄ | Thermal condensation | - | - | Phenol/700 mg L ⁻¹ | 270 (~62.38) | - | [88] |
| CoFe-LDH/ g-C ₃ N ₄ | Coprecipitation method | - | 5 W LED light, >420 nm | TC/40 mg L ⁻¹ | 180 (~83.8) | - | [79] |
| FCCN/LDH | Coprecipitation process | 50 | 300 W Xe lamp | TC/20 mg L ⁻¹ | 120 (~72.13) | 2.314 | [89] |
| g-C ₃ N ₄ / NiZnAl-LDH | Hydrothermal method | 25 | 500 W Xenon lamp, >400 nm | TC/10 mg L ⁻¹ | 120 (>99) | 2.329 | [90] |
| ZnAlS _x @ g-C ₃ N ₄ | Hydrothermal method | 50 | 300 W Xe lamp | TC/20 mg L ⁻¹ | 180 (~94.05) | - | [91] |
| Ag/g-C ₃ N ₄ / CoNi-LDH | Hydrothermal method | 40 | 100 W Xe lamp | TC/30 mg L ⁻¹ | 100 (~86.3) | - | [93] |
| RGO/g-C ₃ N ₄ / NiMgAl LDH | Hydrothermal method | 20 | 250 W mercury lamp | MB/50 mg L ⁻¹ | 75 (~95.14) | 1.8 | [94] |
| LDH/CN/RGO | Hydrothermal method | 50 | 300-W halogen lamp | TC/20 mg L ⁻¹ | 30 (>99) | - | [92] |
| NiFe-LDH/ g-C ₃ N ₄ | Hydrothermal method | 20 | 500 W Xenon lamp, >420 nm | - | 60 (~96.81) | 5.457 | [95] |
| g-C ₃ N ₄ @ NiAl-LDH | Hydrothermal method | 600 | 500W high-pressure Hg lamp. | - | 180 (~99) | - | [96] |
| g-C ₃ N ₄ @ NiFe-LDH | Hydrothermal method | 50 | 500 W Xenon lamp, >420 nm | - | 240 (~99) | 1.52 | [97] |
| g-C ₃ N ₄ / MgZnAl-calcined LDH | Template method | 250 | 300 W Xenon lamp, >420 nm | - | 240 (>99) | - | [98] |
| ZnMgAl LTH/ ZnO/g-C ₃ N ₄ | Stirring strategy | 10 | 300 W Xenon lamp | MB/50 mg L ⁻¹ | 75 (>99) | - | [99] |

Table 2. Cont.

| Photocatalysts | Preparation Strategy | Mass (mg) | Light Source | Target Pollutant/Initial Concentration | Degradation Time (min) and Rate (%) | K_{app}^a [10^{-2} min^{-1}] | Ref. |
|---|--|-----------|---------------------------|--|-------------------------------------|--|-------|
| Co-Al LDH/g-C ₃ N ₄ -CoFe ₂ O ₄ | Stirring strategy | - | 50 W LED lamp | - | - | 2.4 | [100] |
| g-C ₃ N ₄ /ZnFeMMO | Stirring strategy | 25 | 500 W Xenon lamp, >300 nm | Sulfadiazine/5 mg L ⁻¹ | 240 (~96.4) | 1.317 | [76] |
| g-C ₃ N ₄ @LDH/NCQDs | Hydrothermal method | 100 | 300 W Xenon lamp, >400 nm | TC/20 mg L ⁻¹ | 120 (~90) | - | [101] |
| NiFe-LDH/NRGO/g-C ₃ N ₄ | Calcination-electrostatic self-assembly method | 20 | - | RhB/20 mg L ⁻¹ | 120 (~97) | - | [102] |
| ZnCr-LDH/g-C ₃ N ₄ -C(N) | Coprecipitation method | 50 | 500 W Xenon lamp, >400 nm | CR/20 mg L ⁻¹ | 60 (~70) | 1.924 | [57] |
| In ₂ S ₃ /g-C ₃ N ₄ /CoZnAl-LDH | Hydrothermal method | 150 | 300 W Xe lamp, 320–780 nm | MO/50 mg L ⁻¹ | 120 (~90.75) | - | [103] |
| ZnTi/C ₃ N ₄ /Ag LDH | Self-assembly method | 150 | 300 W Xe lamp | Phenol/20 mg L ⁻¹ | 210 (~76.6) | - | [104] |

^a K_{app} represents the reaction rate constant.

5. Conclusions and Outlook

In conclusion, developing LDH/g-C₃N₄ heterojunctions is a successful method for achieving effective photocatalysis for the removal of organic pollution. The separation and transfer of photoinduced charge carriers can be substantially facilitated by the planar configuration and close contact of LDH and g-C₃N₄, which improves photocatalytic performance. For building an LDH/g-C₃N₄ heterojunction with the 2D/2D and suitable band structures, a variety of synthesis techniques have been reported, including electrostatic self-assembly, in situ coprecipitation, hydrothermal, solvothermal, and calcination strategies. An excellent photocatalytic property in the breakdown of organic pollutants may be attributed to the synergistic interaction between LDH and g-C₃N₄. The research investigations on LDH/g-C₃N₄ photocatalysts are still in their early stages, despite the many successes that have been made, and it is clear that more study is required. The following examples of opportunities and difficulties call for greater emphasis and investigation:

- (i) Matching the redox potential of a particular photocatalytic process with the CB (or VB) potential of LDH/g-C₃N₄ photocatalysts is crucial. This is likely to modify the CB (or VB) position of LDHs/g-C₃N₄ to offer high redox potential for a variety of photocatalytic processes since the band structure of the compound is customizable. The precise adjustment technique, however, requires more research.
- (ii) Gaining an in-depth understanding of the transfer mechanism of charge is also crucial. The precise charge transfer pathway and photocatalytic process can be further provided using theoretical calculations and characterization methods [61,105,106] including in situ FTIR, in situ XPS, photo-KPFM, and synchrotron radiation. The search for additional LDH can combine with g-C₃N₄ to improve photocatalytic activity, which is made easier with a greater knowledge of the mechanism.
- (iii) Constructing ultrathin 2D/2D structures is highly worth considering. The ultrathin LDHs and g-C₃N₄ have been suggested as photocatalysts in certain investigations. This is also likely to construct ultrathin LDH/g-C₃N₄ heterojunctions that will enable more rapid photocarrier migration because of the further shortened migration distance and decreased photocarrier recombination.

- (iv) Enhancing the capacity to capture visible or even near-infrared light, which accounts for over half of solar radiation, is strongly advised. Even while LDH/g-C₃N₄ photocatalysts can work with visible light, surface sensitization, doping, band gap correction, and other techniques can help them gather sunlight more effectively.
- (v) Expanding the applications of LDH/g-C₃N₄ photocatalysts in light of their special advantages is essential to creating a sustainable society.
- (vi) Some effective enhancement strategies, such as morphological modulation, loading co-catalysts, interface engineering, doping, and exposing more reactive facets, should be seriously studied to achieve an actual application of LDH/g-C₃N₄ systems.
- (vii) Improving the ability to harness both visible light and near-infrared light, which collectively represent more than 50% of solar irradiation, is paramount. LDH/g-C₃N₄ photocatalysts show potential for efficient operation under visible light, and there are also opportunities to further enhance sunlight harvesting capacity through techniques such as surface sensitization, doping elements, adjusting the band gap, and more.

Looking ahead, this developing field offers both many prospects and difficult problems.

This review is thought to be able to offer some fresh and sophisticated perspectives for directing the logical design of LDH/g-C₃N₄ systems for organic pollution removal. There is no doubt that the LDH/g-C₃N₄ systems will soon have useful industrial applications.

Author Contributions: Conceptualization, J.X., G.D. and W.Q.; writing—original draft preparation, C.D., C.L. and G.L.; writing—review and editing, G.L., D.H. and H.Z. All authors have read and agreed to the published version of the manuscript.

Funding: This work was supported by the National Natural Science Foundation of China (Grant No. 52203110), the Natural Science Foundation of Fujian Province (Grant No. 2023J05052), and the Knowledge Innovation Program of Wuhan-Shuguang Project (Grant No. 2022010801020216).

Data Availability Statement: The data presented in this study are available in this article.

Conflicts of Interest: Author Cheng Du, Jialin Xu, Dayong He and Hao Zhang were employed by the company Shenzhen Mindray Bio-Medical Electronics Co., Ltd. The remaining authors declare that the research was conducted in the absence of any commercial or financial relationships that could be construed as a potential conflict of interest.

References

1. Liu, Z.; Liu, C.; Chen, Z.; Huang, H.; Liu, Y.; Xue, L.; Sun, J.; Wang, X.; Xiong, P.; Zhu, J. Recent advances in two-dimensional materials for hydrovoltaic energy technology. *Exploration* **2023**, *3*, 20220061. [[CrossRef](#)] [[PubMed](#)]
2. Jia, R.; He, C.; Li, Q.; Liu, S.-Y.; Liao, G. Renewable plant-derived lignin for electrochemical energy systems. *Trends Biotechnol.* **2022**, *40*, 1425–1438. [[CrossRef](#)]
3. Li, C.; Jia, R.; Yang, Y.; Liao, G. A Hierarchical Helical Carbon Nanotube Fiber Artificial Ligament. *Adv. Fiber Mater.* **2023**, *5*, 1549–1551. [[CrossRef](#)]
4. Lan, Q.; Jin, S.-J.; Wang, Z.; Li, X.-Y.; Xiong, Y.; Wang, Z.-C.; Liu, S.-S.; Zhang, Z.-M.; Zhao, Q. Design and synthesis of polyoxovanadate-based framework for efficient dye degradation. *Tungsten* **2023**. [[CrossRef](#)]
5. Khan, A.; Nilam, B.; Rukhsar, C.; Sayali, G.; Mandekar, B.; Kadam, A. A review article based on composite graphene @tungsten oxide thin films for various applications. *Tungsten* **2023**, *5*, 391–418. [[CrossRef](#)]
6. Chen, J.; Wang, Y.; Yu, Y.; Wang, J.; Liu, J.; Ihara, H.; Qiu, H. Composite materials based on covalent organic frameworks for multiple advanced applications. *Exploration* **2023**, *3*, 20220144. [[CrossRef](#)]
7. Cheng, Q.; Zhang, G.-K. Enhanced photocatalytic performance of tungsten-based photocatalysts for degradation of volatile organic compounds: A review. *Tungsten* **2020**, *2*, 240–250. [[CrossRef](#)]
8. Lin, J.-H.; Yan, Y.-T.; Qi, J.-L.; Zha, C.-Y. Atomic tailoring-induced deficiency in tungsten oxides for high-performance energy-related devices. *Tungsten* **2023**. [[CrossRef](#)]
9. Qiao, Y.; Sun, C.; Jian, J.; Zhou, T.; Xue, X.; Shi, J.; Che, G.; Liao, G. Efficient removal of organic pollution via photocatalytic degradation over a TiO₂@HKUST-1 yolk-shell nanoreactor. *J. Mol. Liq.* **2023**, *385*, 122383. [[CrossRef](#)]
10. Yao, L.; Sun, C.; Lin, H.; Li, G.; Lian, Z.; Song, R.; Zhuang, S.; Zhang, D. Electrospun Bi-decorated Bi₂Ti₂O₇/TiO₂ flexible carbon nanofibers and their applications on degrading of organic pollutants under solar radiation. *J. Mater. Sci. Technol.* **2023**, *150*, 114–123. [[CrossRef](#)]
11. Liao, G.; Li, C.; Fang, B. Donor-acceptor organic semiconductor heterojunction nanoparticles for efficient photocatalytic H₂ evolution. *Matter* **2022**, *5*, 1635–1637. [[CrossRef](#)]

12. Liao, G.; Fang, B.; Li, C. A high-pressure-tolerant vapor-fed photocatalytic system for efficient water splitting. *Chem Catal.* **2023**, *3*, 100671. [[CrossRef](#)]
13. Ghugal, S.G.; Kumar Tadi, K.; Rani, K.; Mendhe, A.C.; Jeong, Y.; Yoon, J. Improved photocatalytic performance of CdS/ α -Fe₂O₃ heterostructure for anionic dye mineralization and charge storage applications. *J. Mol. Liq.* **2023**, *392*, 123384. [[CrossRef](#)]
14. Duta, A.; Andronic, L.; Enesca, A. The influence of low irradiance and electrolytes on the mineralization efficiency of organic pollutants using the Vis-active photocatalytic tandem CuInS₂/TiO₂/SnO₂. *Catal. Today* **2018**, *300*, 18–27. [[CrossRef](#)]
15. Tao, X.; Ren, J.; Wang, D.; Huang, H.; Li, Y.; Guo, D.; Shan, B.; Liu, Y.; Wang, J.; Zhen, Y.; et al. Refining the d-band center of S-scheme CdIn₂S₄/MnZnFe₂O₄ heterostructures by interfacial electric field with boosting photocatalytic performance. *Chem. Eng. J.* **2023**, *478*, 147347. [[CrossRef](#)]
16. Palani, G.; Apsari, R.; Hanafiah, M.M.; Venkateswarlu, K.; Lakkaboyana, S.K.; Kannan, K.; Shivanna, A.T.; Idris, A.M.; Yadav, C.H. Metal-Doped Graphitic Carbon Nitride Nanomaterials for Photocatalytic Environmental Applications-A Review. *Nanomaterials* **2022**, *12*, 1754. [[CrossRef](#)]
17. Wang, X.; Maeda, K.; Thomas, A.; Takanabe, K.; Xin, G.; Carlsson, J.M.; Domen, K.; Antonietti, M. A metal-free polymeric photocatalyst for hydrogen production from water under visible light. *Nat. Mater.* **2009**, *8*, 76–80. [[CrossRef](#)]
18. Liao, G.; Tao, X.; Fang, B. An innovative synthesis strategy for high-efficiency and defects-switchable-hydrogenated TiO₂ photocatalysts. *Matter* **2022**, *5*, 377–379. [[CrossRef](#)]
19. Li, W.; Sohail, M.; Anwar, U.; Taha, T.A.; Al-Sehemi, A.G.; Muhammad, S.; Al-Ghamdi, A.A.; Amin, M.A.; Palamanit, A.; Ullah, S.; et al. Recent progress in g-C₃N₄-Based materials for remarkable photocatalytic sustainable energy. *Int. J. Hydrog. Energy* **2022**, *47*, 21067–21118. [[CrossRef](#)]
20. Abu-Sari, S.M.; Daud, W.M.A.W.; Patah, M.F.A.; Ang, B.C. A review on synthesis, modification method, and challenges of light-driven H₂ evolution using g-C₃N₄-based photocatalyst. *Adv. Colloid Interface Sci.* **2022**, *307*, 102722. [[CrossRef](#)]
21. Zhang, Q.; Liao, G.; Yang, B.; Zhang, Y.; Ge, G.; Lipovka, A.; Liu, J.; Rodriguez, R.D.; Yang, X.; Jia, X. Structural reorganization of ultrathin g-C₃N₄ nanosheets for significantly boosting wide-spectrum-driven CO₂ photoreduction. *Appl. Surf. Sci.* **2023**, *638*, 157989. [[CrossRef](#)]
22. Tian, F.; Wu, X.; Chen, J.; Sun, X.; Yan, X.; Liao, G. One-step photodeposition of spatially separated CuO_x and MnO_x dual cocatalysts on g-C₃N₄ for enhanced CO₂ photoreduction. *Dalton Trans.* **2023**, *52*, 11934–11940. [[CrossRef](#)] [[PubMed](#)]
23. Tian, F.; Wu, X.; Liu, S.; Gu, Y.; Lin, Z.; Zhang, H.; Yan, X.; Liao, G. Boosting photocatalytic H₂ evolution through interfacial manipulation on a lotus seedpod shaped Cu₂O/g-C₃N₄ p-n heterojunction. *Sustain. Energy Fuels* **2023**, *7*, 786–796. [[CrossRef](#)]
24. Wudil, Y.S.; Ahmad, U.F.; Gondal, M.A.; Al-Osta, M.A.; Almohammed, A.; Sa'id, R.S.; Hrahsheh, F.; Haruna, K.; Mohamed, M.J.S. Tuning of graphitic carbon nitride (g-C₃N₄) for photocatalysis: A critical review. *Arabian J. Chem.* **2023**, *16*, 104542. [[CrossRef](#)]
25. Wang, Q.; Fang, Z.; Zhang, W.; Zhang, D. High-Efficiency g-C₃N₄ Based Photocatalysts for CO₂ Reduction: Modification Methods. *Adv. Fiber Mater.* **2022**, *4*, 342–360. [[CrossRef](#)]
26. Li, Y.; Zhou, M.; Cheng, B.; Shao, Y. Recent advances in g-C₃N₄-based heterojunction photocatalysts. *J. Mater. Sci. Technol.* **2020**, *56*, 1–17. [[CrossRef](#)]
27. Liao, G.; Li, C.; Liu, S.-Y.; Fang, B.; Yang, H. Emerging frontiers of Z-scheme photocatalytic systems. *Trends Chem.* **2022**, *4*, 111–127. [[CrossRef](#)]
28. Li, C.; Cheng, B.; Lu, H.; Ding, G.; Jiang, Z.; Liao, G. Kinetically and Thermodynamically Favorable Ni–Al Layered Double Hydroxide/Ni-Doped Zn_{0.5}Cd_{0.5}S S-Scheme Heterojunction Triggering Photocatalytic H₂ Evolution. *Inorg. Chem.* **2023**, *62*, 6843–6850. [[CrossRef](#)]
29. Ding, G.; Li, C.; Ni, Y.; Chen, L.; Shuai, L.; Liao, G. Layered double hydroxides and their composites as high-performance photocatalysts for CO₂ reduction. *EES Catal.* **2023**, *1*, 369–391. [[CrossRef](#)]
30. Mohapatra, L.; Parida, K. A review on the recent progress, challenges and perspective of layered double hydroxides as promising photocatalysts. *J. Mater. Chem. A* **2016**, *4*, 10744–10766. [[CrossRef](#)]
31. Song, B.; Zeng, Z.; Zeng, G.; Gong, J.; Xiao, R.; Ye, S.; Chen, M.; Lai, C.; Xu, P.; Tang, X. Powerful combination of g-C₃N₄ and LDHs for enhanced photocatalytic performance: A review of strategy, synthesis, and applications. *Adv. Colloid Interface Sci.* **2019**, *272*, 101999. [[CrossRef](#)] [[PubMed](#)]
32. Li, C.; Lu, H.; Ding, G.; Li, Q.; Liao, G. Recent advances on g-C₃N₄-based Z-scheme photocatalysts for organic pollutant removal. *Catal. Sci. Technol.* **2023**, *13*, 2877–2898. [[CrossRef](#)]
33. Sahoo, D.P.; Das, K.K.; Mansingh, S.; Sultana, S.; Parida, K. Recent progress in first row transition metal Layered double hydroxide (LDH) based electrocatalysts towards water splitting: A review with insights on synthesis. *Coordin. Chem. Rev.* **2022**, *469*, 214666. [[CrossRef](#)]
34. Wang, J.; Wang, S. A critical review on graphitic carbon nitride (g-C₃N₄)-based materials: Preparation, modification and environmental application. *Coordin. Chem. Rev.* **2022**, *453*, 214338. [[CrossRef](#)]
35. Luo, B.; Liu, G.; Wang, L. Recent advances in 2D materials for photocatalysis. *Nanoscale* **2016**, *8*, 6904–6920. [[CrossRef](#)]
36. Wang, Q.; O'Hare, D. Recent Advances in the Synthesis and Application of Layered Double Hydroxide (LDH) Nanosheets. *Chem. Rev.* **2012**, *112*, 4124–4155. [[CrossRef](#)] [[PubMed](#)]
37. Ni, J.; Xue, J.; Xie, L.; Shen, J.; He, G.; Chen, H. Construction of magnetically separable NiAl LDH/Fe₃O₄-RGO nanocomposites with enhanced photocatalytic performance under visible light. *Phys. Chem. Chem. Phys.* **2018**, *20*, 414–421. [[CrossRef](#)] [[PubMed](#)]

38. Fan, G.; Li, F.; Evans, D.G.; Duan, X. Catalytic applications of layered double hydroxides: Recent advances and perspectives. *Chem. Soc. Rev.* **2014**, *43*, 7040–7066. [[CrossRef](#)]
39. Xu, Z.P.; Zhang, J.; Adebajo, M.O.; Zhang, H.; Zhou, C. Catalytic applications of layered double hydroxides and derivatives. *Appl. Clay Sci.* **2011**, *53*, 139–150. [[CrossRef](#)]
40. Tonda, S.; Kumar, S.; Bhardwaj, M.; Yadav, P.; Ogale, S. g-C₃N₄/NiAl-LDH 2D/2D Hybrid Heterojunction for High-Performance Photocatalytic Reduction of CO₂ into Renewable Fuels. *ACS Appl. Mater. Interfaces* **2018**, *10*, 2667–2678. [[CrossRef](#)]
41. Abazari, R.; Mahjoub, A.R.; Sanati, S.; Rezvani, Z.; Hou, Z.; Dai, H. Ni–Ti Layered Double Hydroxide@Graphitic Carbon Nitride Nanosheet: A Novel Nanocomposite with High and Ultrafast Sonophotocatalytic Performance for Degradation of Antibiotics. *Inorg. Chem.* **2019**, *58*, 1834–1849. [[CrossRef](#)] [[PubMed](#)]
42. Han, Y.-Y.; Lu, X.-L.; Tang, S.-F.; Yin, X.-P.; Wei, Z.-W.; Lu, T.-B. Metal-Free 2D/2D Heterojunction of Graphitic Carbon Nitride/Graphdiyne for Improving the Hole Mobility of Graphitic Carbon Nitride. *Adv. Energy Mater.* **2018**, *8*, 1702992. [[CrossRef](#)]
43. Li, Y.; Zhang, H.; Liu, P.; Wang, D.; Li, Y.; Zhao, H. Cross-Linked g-C₃N₄/rGO Nanocomposites with Tunable Band Structure and Enhanced Visible Light Photocatalytic Activity. *Small* **2013**, *9*, 3336–3344. [[CrossRef](#)]
44. Low, J.; Yu, J.; Jaroniec, M.; Wageh, S.; Al-Ghamdi, A.A. Heterojunction Photocatalysts. *Adv. Mater.* **2017**, *29*, 1601694. [[CrossRef](#)] [[PubMed](#)]
45. Yang, H. A short review on heterojunction photocatalysts: Carrier transfer behavior and photocatalytic mechanisms. *Mater. Res. Bull.* **2021**, *142*, 111406. [[CrossRef](#)]
46. Xue, C.; An, H.; Shao, G.; Yang, G. Accelerating directional charge separation via built-in interfacial electric fields originating from work-function differences. *Chin. J. Catal.* **2021**, *42*, 583–594. [[CrossRef](#)]
47. Ong, W.-J.; Tan, L.-L.; Chai, S.-P.; Yong, S.-T.; Mohamed, A.R. Surface charge modification via protonation of graphitic carbon nitride (g-C₃N₄) for electrostatic self-assembly construction of 2D/2D reduced graphene oxide (rGO)/g-C₃N₄ nanostructures toward enhanced photocatalytic reduction of carbon dioxide to methane. *Nano Energy* **2015**, *13*, 757–770. [[CrossRef](#)]
48. Liao, G.; Li, C.; Liu, S.-Y.; Fang, B.; Yang, H. Z-scheme systems: From fundamental principles to characterization, synthesis, and photocatalytic fuel-conversion applications. *Phys. Rep.* **2022**, *983*, 1–41. [[CrossRef](#)]
49. Zhang, X.; Xu, Y.; Zhang, X.; Wu, H.; Shen, J.; Chen, R.; Xiong, Y.; Li, J.; Guo, S. Progress on the layer-by-layer assembly of multilayered polymer composites: Strategy, structural control and applications. *Prog. Polym. Sci.* **2019**, *89*, 76–107. [[CrossRef](#)]
50. Zhu, B.; Xia, P.; Ho, W.; Yu, J. Isoelectric point and adsorption activity of porous g-C₃N₄. *Appl. Surf. Sci.* **2015**, *344*, 188–195. [[CrossRef](#)]
51. Yang, Y.J.; Li, W. Ultrasonic assisted coating of multiwalled carbon nanotubes with NiFe-layered double hydroxide for improved electrocatalytic oxygen reduction. *J. Electroanal. Chem.* **2018**, *823*, 499–504. [[CrossRef](#)]
52. Mao, N.; Zhou, C.H.; Tong, D.S.; Yu, W.H.; Cynthia Lin, C.X. Exfoliation of layered double hydroxide solids into functional nanosheets. *Appl. Clay Sci.* **2017**, *144*, 60–78. [[CrossRef](#)]
53. Tahir, M.; Mansoor, R. Constructing Highly Stable CoAl-LDH-Coupled g-C₃N₄ 2D/2D Heterojunctions for Solar Energy-Driven Conversion of Flared Gas to Syngas through Dry-/Bireforming of Methane. *Energy Fuels* **2023**, *37*, 5241–5256. [[CrossRef](#)]
54. Chen, L.; Luque, R.; Li, Y. Controllable design of tunable nanostructures inside metal–organic frameworks. *Chem. Soc. Rev.* **2017**, *46*, 4614–4630. [[CrossRef](#)] [[PubMed](#)]
55. Niu, J.; Qian, H.; Liu, J.; Liu, H.; Zhang, P.; Duan, E. Process and mechanism of toluene oxidation using Cu_{1-y}Mn₂Ce_yO_x/sepiolite prepared by the co-precipitation method. *J. Hazard. Mater.* **2018**, *357*, 332–340. [[CrossRef](#)] [[PubMed](#)]
56. Theiss, F.L.; Ayoko, G.A.; Frost, R.L. Synthesis of layered double hydroxides containing Mg²⁺, Zn²⁺, Ca²⁺ and Al³⁺ layer cations by co-precipitation methods—A review. *Appl. Surf. Sci.* **2016**, *383*, 200–213. [[CrossRef](#)]
57. Liu, J.; Li, J.; Bing, X.; Ng, D.H.L.; Cui, X.; Ji, F.; Kionga, D.D. ZnCr-LDH/N-doped graphitic carbon-incorporated g-C₃N₄ 2D/2D nanosheet heterojunction with enhanced charge transfer for photocatalysis. *Mater. Res. Bull.* **2018**, *102*, 379–390. [[CrossRef](#)]
58. Yuan, X.; Li, W. Graphitic-C₃N₄ modified ZnAl-layered double hydroxides for enhanced photocatalytic removal of organic dye. *Appl. Clay Sci.* **2017**, *138*, 107–113. [[CrossRef](#)]
59. Shi, W.; Song, S.; Zhang, H. Hydrothermal synthetic strategies of inorganic semiconducting nanostructures. *Chem. Soc. Rev.* **2013**, *42*, 5714–5743. [[CrossRef](#)]
60. Merzari, F.; Goldfarb, J.; Andreottola, G.; Mimmo, T.; Volpe, M.; Fiori, L. Hydrothermal Carbonization as a Strategy for Sewage Sludge Management: Influence of Process Withdrawal Point on Hydrochar Properties. *Energies* **2020**, *3*, 2890. [[CrossRef](#)]
61. Li, C.; Liu, X.; Ding, G.; Huo, P.; Yan, Y.; Yan, Y.; Liao, G. Interior and Surface Synergistic Modifications Modulate the SnNb₂O₆/Ni-Doped ZnIn₂S₄ S-Scheme Heterojunction for Efficient Photocatalytic H₂ Evolution. *Inorg. Chem.* **2022**, *61*, 4681–4689. [[CrossRef](#)] [[PubMed](#)]
62. Xu, X.; Wang, Y.; Zhang, D. A novel strategy of hydrothermal in-situ grown bismuth based film on epoxy resin as recyclable photocatalyst for photodegrading antibiotics and sterilizing microorganism. *Sep. Purif. Technol.* **2022**, *290*, 120842. [[CrossRef](#)]
63. Xu, Y.; Liu, T.; Li, Y.; Liu, Y.; Ge, F. Nanostructure Design and Catalytic Performance of Mo/ZnAl-LDH in Cationic Orchid X-BL Removal. *Materials* **2018**, *11*, 2390. [[CrossRef](#)] [[PubMed](#)]
64. Liu, X.; Liang, J.; Song, X.; Yang, H.; Li, X.; Dai, H.; Song, Y.; Liu, Y.; Hu, J.; Pan, X.; et al. Enhanced water dissociation performance of graphitic-C₃N₄ assembled with ZnCr-layered double hydroxide. *Chem. Eng. J.* **2018**, *337*, 560–566. [[CrossRef](#)]

65. Wu, Y.; Wang, H.; Sun, Y.; Xiao, T.; Tu, W.; Yuan, X.; Zeng, G.; Li, S.; Chew, J.W. Photogenerated charge transfer via interfacial internal electric field for significantly improved photocatalysis in direct Z-scheme oxygen-doped carbon nitrogen/CoAl-layered double hydroxide heterojunction. *Appl. Catal. B Environ.* **2018**, *227*, 530–540. [CrossRef]
66. Gupta, S.; Fernandes, R.; Patel, R.; Spreitzer, M.; Patel, N. A review of cobalt-based catalysts for sustainable energy and environmental applications. *Appl. Catal. A Gen.* **2023**, *661*, 119254. [CrossRef]
67. Triolo, C.; Xu, W.; Petrovičová, B.; Pinna, N.; Santangelo, S. Evaluation of Entropy-Stabilized (Mg_{0.2}Co_{0.2}Ni_{0.2}Cu_{0.2}Zn_{0.2})O Oxides Produced via Solvothermal Method or Electrospinning as Anodes in Lithium-Ion Batteries. *Adv. Funct. Mater.* **2022**, *32*, 2202892. [CrossRef]
68. Lai, J.; Niu, W.; Luque, R.; Xu, G. Solvothermal synthesis of metal nanocrystals and their applications. *Nano Today* **2015**, *10*, 240–267. [CrossRef]
69. Mruthunjayappa, M.H.; Kotrappanavar, N.S.; Mondal, D. New prospects on solvothermal carbonisation assisted by organic solvents, ionic liquids and eutectic mixtures—A critical review. *Prog. Mater. Sci.* **2022**, *126*, 100932. [CrossRef]
70. Zhang, L.; Li, L.; Sun, X.; Liu, P.; Yang, D.; Zhao, X. ZnO-Layered Double Hydroxide@Graphitic Carbon Nitride Composite for Consecutive Adsorption and Photodegradation of Dyes under UV and Visible Lights. *Materials* **2016**, *9*, 927. [CrossRef]
71. Ahmed, N.; Morikawa, M.; Izumi, Y. Photocatalytic conversion of carbon dioxide into methanol using optimized layered double hydroxide catalysts. *Catal. Today* **2012**, *185*, 263–269. [CrossRef]
72. Nong, J.; Jin, Y.; Tan, J.; Ma, H.; Lian, Y. Construction of NiCo-LDH/g-C₃N₄ heterojunctions as efficient photocatalysts for enhanced degradation of tetracycline hydrochloride and hydrogen evolution. *New J. Chem.* **2022**, *46*, 22830–22840. [CrossRef]
73. Li, C.; Wei, M.; Evans, D.G.; Duan, X. Layered Double Hydroxide-based Nanomaterials as Highly Efficient Catalysts and Adsorbents. *Small* **2014**, *10*, 4469–4486. [CrossRef]
74. Yang, Z.; Wang, F.; Zhang, C.; Zeng, G.; Tan, X.; Yu, Z.; Zhong, Y.; Wang, H.; Cui, F. Utilization of LDH-based materials as potential adsorbents and photocatalysts for the decontamination of dyes wastewater: A review. *RSC Adv.* **2016**, *6*, 79415–79436. [CrossRef]
75. Van Vaerenbergh, B.; De Vlieger, K.; Claeys, K.; Vanhoutte, G.; De Clercq, J.; Vermeir, P.; Verberckmoes, A. The effect of the hydrotalcite structure and nanoparticle size on the catalytic performance of supported palladium nanoparticle catalysts in Suzuki cross-coupling. *Appl. Catal. A Gen.* **2018**, *550*, 236–244. [CrossRef]
76. Di, G.; Zhu, Z.; Huang, Q.; Zhang, H.; Zhu, J.; Qiu, Y.; Yin, D.; Zhao, J. Targeted modulation of g-C₃N₄ photocatalytic performance for pharmaceutical pollutants in water using ZnFe-LDH derived mixed metal oxides: Structure-activity and mechanism. *Sci. Total Environ.* **2019**, *650*, 1112–1121. [CrossRef]
77. Shi, J.; Li, S.; Wang, F.; Gao, L.; Li, Y.; Zhang, X.; Lu, J. 2D/2D g-C₃N₄/MgFe MMO nanosheet heterojunctions with enhanced visible-light photocatalytic H₂ production. *J. Alloys Compd.* **2018**, *769*, 611–619. [CrossRef]
78. Ali Khan, A.; Tahir, M. Constructing S-Scheme Heterojunction of CoAlLa-LDH/g-C₃N₄ through Monolayer Ti₃C₂-MXene to Promote Photocatalytic CO₂ Re-forming of Methane to Solar Fuels. *ACS Appl. Energy Mater.* **2022**, *5*, 784–806. [CrossRef]
79. Li, M.; Chen, M.; Lee, S.L.J.; Lin, S. Facile fabrication of a 2D/2D CoFe-LDH/g-C₃N₄ nanocomposite with enhanced photocatalytic tetracycline degradation. *Environ. Sci. Poll. Res.* **2023**, *30*, 4709–4720. [CrossRef]
80. Gandamalla, A.; Manchala, S.; Verma, A.; Fu, Y.-P.; Shanker, V. Microwave-assisted synthesis of ZnAl-LDH/g-C₃N₄ composite for degradation of antibiotic ciprofloxacin under visible-light illumination. *Chemosphere* **2021**, *283*, 131182. [CrossRef]
81. Cheshmeh Soltani, R.D.; Abolhasani, E.; Mashayekhi, M.; Jorfi, N.; Boczkaj, G.; Khataee, A. Degradation of tetracycline antibiotic utilizing light driven-activated oxone in the presence of g-C₃N₄/ZnFe LDH binary heterojunction nanocomposite. *Chemosphere* **2022**, *303*, 135201. [CrossRef] [PubMed]
82. Sun, D.; Chi, D.; Yang, Z.; Xing, Z.; Yin, J.; Li, Z.; Zhu, Q.; Zhou, W. Mesoporous g-C₃N₄/Zn-Ti LDH laminated van der Waals heterojunction nanosheets as remarkable visible-light-driven photocatalysts. *Int. J. Hydrog. Energy* **2019**, *44*, 16348–16358. [CrossRef]
83. Xu, H.; Shan, C.; Wu, X.; Sun, M.; Huang, B.; Tang, Y.; Yan, C.-H. Fabrication of layered double hydroxide microcapsules mediated by cerium doping in metal-organic frameworks for boosting water splitting. *Energy Environ. Sci.* **2020**, *13*, 2949–2956. [CrossRef]
84. Yuan, N.; Deng, Y.-R.; Wang, S.-H.; Gao, L.; Yang, J.-L.; Zou, N.-C.; Liu, B.-X.; Zhang, J.-Q.; Liu, R.-P.; Zhang, L. Towards superior lithium-sulfur batteries with metal-organic frameworks and their derivatives. *Tungsten* **2022**, *4*, 269–283. [CrossRef]
85. Huang, X.; Xu, X.; Yang, R.; Fu, X. Synergetic adsorption and photocatalysis performance of g-C₃N₄/Ce-doped MgAl-LDH in degradation of organic dye under LED visible light. *Colloid. Surf. A Physicochem. Eng. Asp.* **2022**, *643*, 128738. [CrossRef]
86. Huang, Z.; Song, H.; Li, A.; An, Z.; Zhang, K.; Xiang, X.; Shu, X.; He, J. Z-Scheme ZnM-LDHs/g-C₃N₄ (M = Al, Cr) Photocatalysts: Their Desulfurization Performance and Mechanism for Model Oil with Air. *Energy Fuels* **2020**, *34*, 14676–14687. [CrossRef]
87. Beigi, F.; Mahjoub, A.R.; Khavar, A.H.C. Design and synthesis of Bi-doped NiAl-LDH/g-C₃N₄ heterostructure; a novel 2D/2D system for simultaneous enhanced photocatalytic degradation and fluorescence sensing of ciprofloxacin. *Appl. Surf. Sci.* **2023**, *637*, 157972. [CrossRef]
88. Tripathi, A.; Hussain, C.M. ZnAl-LDH and B-impregnated polymeric semiconductor (g-C₃N₄) for solar light-driven photocatalysis to treat phenolic effluent. *Sustain. Mater. Technol.* **2021**, *28*, e00266. [CrossRef]
89. Hu, J.; Sun, C.; Wu, L.-X.; Zhao, G.-Q.; Liu, H.-Y.; Jiao, F.-P. Halogen doped g-C₃N₄/ZnAl-LDH hybrid as a Z-scheme photocatalyst for efficient degradation for tetracycline in seawater. *Sep. Purif. Technol.* **2023**, *309*, 123047. [CrossRef]
90. Feng, X.; Li, X.; Su, B.; Ma, J. Hydrothermal construction of flower-like g-C₃N₄/NiZnAl-LDH S-scheme heterojunction with oxygen vacancies for enhanced visible-light triggered photocatalytic performance. *J. Alloys Compd.* **2022**, *922*, 166098. [CrossRef]

91. Hu, J.; Zhao, G.-Q.; Wu, L.-X.; Sun, C.; Long, X.; Long, X.-Q.; Jiao, F.-P. Designing and Fabricating a Vulcanized ZnAl LDH-Modified g-C₃N₄ Heterojunction for Enhanced Visible-Light-Driven Photocatalytic Degradation Activity. *Ind. Eng. Chem. Res.* **2022**, *61*, 15225–15239. [[CrossRef](#)]
92. Jo, W.-K.; Tonda, S. Novel CoAl-LDH/g-C₃N₄/RGO ternary heterojunction with noTable 2D/2D/2D configuration for highly efficient visible-light-induced photocatalytic elimination of dye and antibiotic pollutants. *J. Hazard. Mater.* **2019**, *368*, 778–787. [[CrossRef](#)] [[PubMed](#)]
93. Fazaeli, R.; Aliyan, H.; Richeson, D.; Li, Y. A comparison increasing the photodegradation power of a Ag/g-C₃N₄/CoNi-LDH nanocomposite: Photocatalytic activity toward water treatment. *J. Environ. Sci.* **2023**. [[CrossRef](#)]
94. Bhuvanewari, K.; Palanisamy, G.; Pazhanivel, T.; Maiyalagan, T. r-GO supported g-C₃N₄/NiMgAl layered triple hydroxide hybrid as a Visible Light photocatalyst for organic dye removal. *Colloid. Surf. A Physicochem. Eng. Asp.* **2020**, *602*, 125078. [[CrossRef](#)]
95. Zhao, G.-Q.; Long, X.; Hu, J.; Zou, J.; Jiao, F.-P.; Research, E.C. NiFe-layered double hydroxides as a novel hole repository layer for reinforced visible-light photocatalytic activity for degradation of refractory pollutants. *Ind. Eng. Chem. Res.* **2021**, *60*, 13834–13845. [[CrossRef](#)]
96. Salehi, G.; Abazari, R.; Mahjoub, A.R. Visible-Light-Induced Graphitic-C₃N₄@Nickel-Aluminum Layered Double Hydroxide Nanocomposites with Enhanced Photocatalytic Activity for Removal of Dyes in Water. *Inorg. Chem.* **2018**, *57*, 8681–8691. [[CrossRef](#)]
97. He, Y.; Zhou, S.; Wang, Y.; Jiang, G.; Jiao, F. Fabrication of g-C₃N₄@NiFe-LDH heterostructured nanocomposites for highly efficient photocatalytic removal of rhodamine B. *J. Mater. Sci.: Mater. Electron.* **2021**, *32*, 21880–21896. [[CrossRef](#)]
98. Yu, Y.; Chen, D.; Xu, W.; Fang, J.; Sun, J.; Liu, Z.; Chen, Y.; Liang, Y.; Fang, Z. Synergistic adsorption-photocatalytic degradation of different antibiotics in seawater by a porous g-C₃N₄/calcined-LDH and its application in synthetic mariculture wastewater. *J. Hazard. Mater.* **2021**, *416*, 126183. [[CrossRef](#)]
99. Bhuvanewari, K.; Palanisamy, G.; Bharathi, G.; Pazhanivel, T.; Upadhyaya, I.R.; Kumari, M.L.A.; Rajesh, R.P.; Govindasamy, M.; Ghfar, A.; Al-Shaalan, N.H. Visible light driven reduced graphene oxide supported ZnMgAl LTH/ZnO/g-C₃N₄ nanohybrid photocatalyst with notable two-dimension formation for enhanced photocatalytic activity towards organic dye degradation. *Environ. Res.* **2021**, *197*, 111079. [[CrossRef](#)]
100. Sheikhpour, H.; Saljooqi, A.; Shamspur, T.; Mostafavi, A. Co-Al Layered double hydroxides decorated with CoFe₂O₄ nanoparticles and g-C₃N₄ nanosheets for efficient photocatalytic pesticide degradation. *Environ. Technol. Innov.* **2021**, *23*, 101649. [[CrossRef](#)]
101. Arjomandi-Behzad, L.; Alinejad, Z.; Zandragh, M.R.; Golmohamadi, A.; Vojoudi, H. Facile synthesis of hollow spherical g-C₃N₄@LDH/NCQDs ternary nanostructure for multifunctional antibacterial and photodegradation activities. *iScience* **2023**, *26*, 106213. [[CrossRef](#)] [[PubMed](#)]
102. Nayak, S.; Parida, K.M. Deciphering Z-scheme Charge Transfer Dynamics in Heterostructure NiFe-LDH/N-rGO/g-C₃N₄ Nanocomposite for Photocatalytic Pollutant Removal and Water Splitting Reactions. *Sci. Rep.* **2019**, *9*, 2458. [[CrossRef](#)] [[PubMed](#)]
103. Sun, X.; Li, L.; Hu, T.; Lian, Q.; Liu, Y.; Hou, J.; Yu, Y.; Cao, Y.; Ma, F. In₂S₃/g-C₃N₄/CoZnAl-LDH composites with the lamellar dual S-scheme heterostructure and its enhanced photocatalytic performance. *Colloid. Surf. A Physicochem. Eng. Asp.* **2023**, *658*, 130744. [[CrossRef](#)]
104. Lestari, P.R.; Takei, T.; Kumada, N. Novel ZnTi/C₃N₄/Ag LDH heterojunction composite for efficient photocatalytic phenol degradation. *J. Solid State Chem.* **2021**, *294*, 121858. [[CrossRef](#)]
105. Gao, X.; Chen, J.; Che, H.; Ao, Y.; Wang, P. Rationally constructing of a novel composite photocatalyst with multi charge transfer channels for highly efficient sulfamethoxazole elimination: Mechanism, degradation pathway and DFT calculation. *Chem. Eng. J.* **2021**, *426*, 131585. [[CrossRef](#)]
106. Bai, S.; Jiang, J.; Zhang, Q.; Xiong, Y. Steering charge kinetics in photocatalysis: Intersection of materials syntheses, characterization techniques and theoretical simulations. *Chem. Soc. Rev.* **2015**, *44*, 2893–2939. [[CrossRef](#)]

Disclaimer/Publisher's Note: The statements, opinions and data contained in all publications are solely those of the individual author(s) and contributor(s) and not of MDPI and/or the editor(s). MDPI and/or the editor(s) disclaim responsibility for any injury to people or property resulting from any ideas, methods, instructions or products referred to in the content.